High-pressure phase transformation and metastable phases of a Si_<0.29>Ge_<0.71> alloy using a diamond anvil cell

Ikoma, Yoshifumi
Department of Materials, Kyushu University

Sato, Yuma
Department of Materials, Kyushu University

Kadobayashi, Hirokazu
Japan Synchrotron Radiation Research Institute

Kawaguchi-Imada, Saori
Japan Synchrotron Radiation Research Institute

他

出版情報：Applied Physics Letters. 127 (7), pp.071901-, 2025-08-18. AIP Publishing
バージョン：

High-pressure phase transformation and metastable phases of a $Si_{0.29}Ge_{0.71}$ alloy using a diamond anvil cell

Yoshifumi Ikoma[1,a], Yuma Sato,[1] Hirokazu Kadobayashi,[2] Saori Kawaguchi-Imada,[2,3,4] Seung Zeon Han,[5] Eun-Ae Choi,[5,a] and Yasutomo Arai[6]

[1]*Department of Materials, Kyushu University, Fukuoka 819-0395, Japan*
[2]*Japan Synchrotron Radiation Research Institute, Sayo, Hyogo 679-5198, Japan*
[3]*DECTRIS Japan, Himeji, Hyogo 670-0965, Japan*
[4]*Faculty of Materials for Energy, Shimane University, Matsue, Shimane 690-8504, Japan*
[5]*Extreme Materials Research Institute, Korea Institute of Materials Science, Changwon, Gyeongnam 51508, Republic of Korea*
[6]*Japan Aerospace Exploration Agency, Tsukuba, Ibaraki 305-8505, Japan*

We investigated the high-pressure phase transformation of a $Si_{0.29}Ge_{0.71}$ alloy grown by a traveling liquidus-zone (TLZ) method. The TLZ-grown $Si_{0.29}Ge_{0.71}$ alloy was subjected to high pressures of up to ~15 GPa using a diamond anvil cell. In situ synchrotron X-ray diffraction (XRD) and micro-Raman measurements revealed the appearance of a tetragonal β-Sn phase at 12.1 GPa. A weakened residual diamond-cubic (dc) diffraction peak together with dominant β-Sn peaks was present at 15.2 GPa. Upon depressurization, a metastable rhombohedral r8 phase appeared at 8.4 GPa. When depressurized to ambient pressure, the XRD profile showed an almost body-centered-cubic bc8 phase with residual weak r8 and dc diffraction peaks. No appreciable Raman peaks were observed upon depressurization down to 4.1 GPa, but weak peaks appeared at ~283 cm^{-1} and ~396 cm^{-1} at ambient pressure. Theoretical calculations based on density functional perturbation theory indicated that the observed peaks were not related to bc8, but rather to hexagonal diamond (hd). These results indicate that a bc8 → hd phase transformation was induced by laser heating during the Raman measurement.

[a)]Authors to whom correspondence should be addressed: ikoma@zaiko.kyushu-u.ac.jp and eunae.choi@kims.re.kr

Group IV semiconductor allotropes have attracted much attention because they are expected to exhibit interesting physical properties that cannot be achieved in a diamond-cubic (dc) crystal structure.[1,2] The allotropes of Si and Ge are obtained through phase transformations under high pressure.[3] When Si and Ge crystals are subjected to high pressure, Si-I/Ge-I with the dc structure transforms to a tetragonal (β-Sn) Si-II/Ge-II phase. The pressure of the Si-I → Si-II phase transformation is at ~10 GPa under hydrostatic conditions,[3] but it decreases to 0.3 GPa under plastic strain for Si nanoparticles with a size of 100 nm.[4] Upon depressurization, Si-II and Ge-II transform to metastable Si-III (bc8) through Si-XII (r8), and Ge-III (st12) which does not further transform to bc8-Ge, respectively.[3] Since Si-III, Si-XII, and Ge-III have different bandgaps of 30 meV,[5] 0.24 eV,[6] and 0.59 eV,[7] respectively, the metastable phases of SiGe alloys can cover a wider range of bandgaps.

The dc-SiGe alloys have been used in strained Si channel metal-oxide-semiconductor field-effect transistors,[8] quantum wells using Si/SiGe/Si heterostructures,[9] and thermoelectric devices.[10] The dc-$Si_{1-x}Ge_x$ alloys exhibit an indirect bandgap ranging from 0.66 to 1.12 eV with Ge atomic composition x,[11] while a direct bandgap can be realized in a hexagonal structure for $x > 0.65$.[12] The high-pressure phase transformation of SiGe alloys has been studied both experimentally[13] and theoretically.[14–17] Recently, Serghiou *et al*.[18] reported the formation of metastable bc8/st12 phases of SiGe alloys obtained via a high-pressure and high-temperature process utilizing a multianvil system. They also reported the synthesis of hexagonal SiGe alloys using multianvil and laser-heated diamond anvil cell methods.[19] High pressure phase transformation and formation of bc8/r8 phases of $Si_{0.8}Ge_{0.2}$ were reported by Gerin *et al*.[20] The formation of bc8-$Si_{0.5}Ge_{0.5}$ was achieved by severe plastic deformation using high-pressure torsion.[21] A theoretical study predicts that st12-$Si_{1-x}Ge_x$ exhibits a direct bandgap when $x \approx 0.84$.[22] However, the detailed phase transformations and the formation of metastable phases in SiGe alloys are not yet fully understood. In this study, we investigated the high-pressure phase transformation of a $Si_{0.29}Ge_{0.71}$ alloy using synchrotron X-ray diffraction (XRD) and micro-Raman measurements using a diamond anvil cell (DAC).

The $Si_{0.29}Ge_{0.71}$ alloy crystal was prepared by the traveling liquidus-zone method (TLZ).[23] The bulk-polycrystalline $Si_{0.29}Ge_{0.71}$ piece was characterized by Raman spectroscopy (micro-Raman system HR 800, HORIBA) using a semiconductor laser at a wavelength of 488 nm and a laser output power of 10 mW. The alloy crystal was crushed into a powder in a mortar, and then placed in a DAC with a stainless gasket. The culet size of the diamond anvils was 0.5 mm. Helium was used as a pressure-transmitting medium to achieve nearly hydrostatic conditions. The high-pressure DAC experiments were performed at BL10XU of SPring-8, where XRD profiles and micro-Raman spectra can be obtained simultaneously.[24] The wavelengths of XRD and micro-Raman measurements were set at 0.0414 nm and 532 nm, respectively. The laser power was set to 5–8 mW for the micro-Raman measurements. The X-ray beam was collimated to a diameter of 60 μm. The DAC was remotely pressurized and depressurized by a gas-driven membrane. Pressurization and depressurization were performed incrementally while holding at each pressure. During each holding period, a Raman measurement was taken first, followed by an XRD profile. The pressure was determined by conventional ruby fluorescence measurements.[25] All the DAC experiments and measurements were carried out at room temperature. The diffraction patterns obtained by a flat-panel detector were converted into one-dimensional profiles using IPAnalyzer.[26] The changes in lattice constants and cell volumes were determined by PDIndexer[26] and Le Bail analysis on the Jana2006 software.[27] To provide a deeper understanding of the experimental results, we performed first-principles calculations of the zone-center phonon frequencies for the r8, bc8, and 2H hexagonal diamond (hd) phases of $Si_{0.3}Ge_{0.7}$, with the Ge concentration comparable to that used in this study. These calculations were carried out using the density functional perturbation theory (DFPT) within the Vienna Ab-Initio Simulation Package (VASP).[28,29] The Perdew–Burke–Ernzerhof exchange correlation functional (PBE-GGA)[30] and the projector augmented wave (PAW) method[31,32] were employed. The Si and Ge pseudopotentials included Si $3s^2 3p^2$ and Ge $4s^2 4p^2$ as their respective valence electrons. A wavefunction energy cutoff of 300 eV was applied. The convergence criteria for electronic self-consistency and structural

relaxation were set to 10^{-8} eV and 10^{-4} eV/Å, respectively. Alloying effects were considered using the special quasi-random structure (SQS),[33] generated through Monte Carlo samplings within the Advanced Theoretical Alloy Toolkit (ATAT-mcsqs).[34] The structural and atomic relaxations were performed on an 80-atom SQS cell, with 6×3×2 and 5×5×1 Monkhorst-Pack (MP)[35] k-meshes applied to the r8-$Si_{0.3}Ge_{0.7}$ phase at 5.6 GPa, and bc8- and hd-$Si_{0.3}Ge_{0.7}$ phases at ambient pressure, respectively. The cell volume was fixed at 18.5 Å^3/atom for r8-$Si_{0.3}Ge_{0.7}$ based on the lattice constant shown in the supplementary material (Fig. S1). The cell volumes for bc8-$Si_{0.3}Ge_{0.7}$ and hd-$Si_{0.3}Ge_{0.7}$ were fixed at 20.0 Å^3/atom and 21.7 Å^3/atom, respectively, in accordance with Vegard's law,[36] based on the experimental lattice parameters of bc8-Si, bc8-Ge, hd(2H)-Si, and hd(2H)-Ge.[5,37–39]

Figures 1(a) and 1(b) show the XRD profile of the $Si_{0.29}Ge_{0.71}$ powder and the Raman spectrum of the bulk-crystal $Si_{0.29}Ge_{0.71}$ sample, respectively, at atmospheric pressure. The diffraction peaks in Fig. 1(a) correspond to the dc structure with a lattice constant of 0.5586 nm, which is in good agreement with that reported by Dismukes *et al*.[40,41] The Raman peaks in Fig. 1(b) at 293, 406, and 474 cm^{-1} correspond to Ge–Ge, Si–Ge, and Si–Si Raman peaks with the dc structure for $x \sim 0.7$.[42,43] Some weak peaks at 420–470 cm^{-1} are associated with local vibrational modes (LVM) in Ge-rich SiGe alloys.[44]

Figures 2(a) and 2(b) show the changes in the XRD profiles and Raman spectra, respectively, of the $Si_{0.29}Ge_{0.71}$ powder upon pressurization. The XRD profiles in Fig. 2(a) show that the diffraction peaks corresponding to the dc structure shift to higher diffraction angles as the pressure increases. The Raman peaks in Fig. 2(b) corresponding to the Ge–Ge and Si–Ge modes are also shifted to higher wavenumbers. Weak diffraction peaks at $2\theta \sim 9.8°$ and 10.1° corresponding to a β-Sn structure and the diffraction peaks with the dc structure coexist when the pressure increases to 12.1 GPa, as shown in Fig. 2(a). The intensities of the diffraction peaks corresponding to β-Sn and dc structures increase and decrease, respectively, with increasing pressure. A weakened residual dc peak at ~7.7° together with dominant β-Sn peaks is present at 15.2 GPa. The coexistence of dc and β-Sn phases during pressurization in Fig. 2 is similar to

the case of Si, Ge (Ref. 3), and SiGe alloys.[13,20] The phase transformation pressure from dc to β-Sn of the $Si_{0.29}Ge_{0.71}$ alloy (~12 GPa) shown in Fig. 2 is higher than that of pure Si and Ge. The pressure of dc → β-Sn phase transformation of $Si_{1-x}Ge_x$ alloys has nonlinear dependence on the concentration, because the disordered atomic arrangements in the solid solution SiGe alloys favors the stability of the dc structure.[13,14]

Figure 3 shows the fitting curve of a second-order Birch-Murnaghan (BM2) equation of state[45] for relative volume changes of the dc phase. The bulk modulus K obtained from BM2 is 82.4(3) GPa. The obtained K value follows a linear relationship between that of Si (~100 GPa)[46,47] and Ge (~75 GPa),[48] and is lower than that of $Si_{0.8}Ge_{0.2}$ (92 GPa).[20]

Figures 4(a) and 4(b) show the XRD and Raman spectra upon depressurization, respectively. The residual dc peak at ~7.7° and intense β-Sn peaks are present at 15.4 GPa, as shown in Fig. 4(a). The β-Sn diffraction peaks become weak and shift to lower diffraction angles with decreasing pressure. New diffraction peaks corresponding to rhombohedral r8 appear at 8.4 GPa. The changes in the lattice constants of the r8 phase is shown in the supplementary material (Fig. S1). When depressurized to ambient pressure, the XRD profile includes bc8 and residual r8 and dc peaks. The lattice constant of the bc8 phase at ambient pressure is estimated to be 0.684 nm, which is in good agreement with that of bc8-$Si_{0.3}Ge_{0.7}$ (0.6843 nm), calculated using Vegard's law based on 0.6636 nm and 0.6932 nm for bc8-Si and bc8-Ge, respectively.[37] The estimated lattice constant of the r8 phase at ambient pressure also closely follows Vegard's law, as shown in the supplementary material (Fig. S2). No appreciable Raman peak is observed up to 3.1 GPa as shown in Fig. 4(b). A weak Raman peak at ~300 cm^{-1} appears as the pressure decreases down to 3.1 GPa, and weak broad peaks centered at ~283 cm^{-1} and ~396 cm^{-1} are present at ambient pressure.

Figure 5(a) shows the DFPT calculations of the Raman-active mode frequencies for the r8-$Si_{0.3}Ge_{0.7}$ phase at 5.6 GPa. The Raman spectra of the r8 structure is expected to exhibit significantly broader features spanning a wide frequency range. The Raman frequencies of bc8- and hd-$Si_{0.3}Ge_{0.7}$ at ambient pressure, as calculated using DFPT, are presented in Fig. 5(b) and

compared with the experimental Raman peak positions extracted from Fig. 4(b). For bc8-$Si_{0.3}Ge_{0.7}$, a significant number of Raman modes are present at around 235, 270, 330, and 365 cm^{-1}, which differ notably from the experimental peaks at ~283 and ~396 cm^{-1} under ambient pressure. In contrast, the theoretical Raman modes for hd-$Si_{0.3}Ge_{0.7}$ are primarily located around 280 and 400 cm^{-1}, reasonably matching the experimental results. To facilitate a more accurate comparison between the experimental data and the theoretical calculations, we also calculated the Raman intensity for hd-$Si_{0.3}Ge_{0.7}$ as shown in Fig. 5(c). The maxima of the Raman spectrum were calculated at 285 and 396 cm^{-1}, which align well with the experimentally observed peaks at ~283 and ~396 cm^{-1}.

As shown in Figs. 4(b), 5(b), and 5(c), the experimental and theoretical Raman peak positions corresponding to the hd phase are incompatible with the presence of the bc8 phase, as indicated by the XRD profile in Fig. 4(a). The observed discrepancy indicates that the bc8 → hd phase transformation occurred during the Raman measurement. The phase transformation from bc8 to hd is often observed by annealing at ~200 °C in the case of Si.[49–51] The bc8-Ge phase is unstable at ambient pressure and transforms to hd-Ge at room temperature.[37] These results indicate that bc8-$Si_{0.29}Ge_{0.71}$ easily transforms to the hd phase due to laser heating. No appreciable diffraction peaks of the hd phase in Fig. 4(a) can be attributed to the fact that the area transformed from bc8 to hd by laser heating during micro-Raman measurements is ~50 μm^2, whereas the area in the XRD measurements is ~2.8×10^3 μm^2. The Raman peak corresponding to the r8 phase was not clearly observed during depressurization in Fig. 4(b), which is likely due to severe peak broadening that rendered it undetectable within the spectral resolution. This broadening can be attributed to several factors. First, a SiGe alloy system introduces significant atomic-scale disorder due to the random substitution of Si and Ge atoms. This random atomic arrangement disrupts the periodic lattice potential and results in a distribution of local bonding environments, leading to a natural broadening of phonon modes. The Raman-active mode frequencies of r8 shown in Fig. 5(a) is a strong indication of increased structural disorder in the r8-$Si_{0.3}Ge_{0.7}$ phase. The pair distribution function analysis in the

supplementary material (Fig. S3 and Table S1) also confirms that r8-$Si_{0.3}Ge_{0.7}$ phase is the most disordered among the three phases. Second, the coexistence of the metallic β-Sn phase may have introduced electronic screening and optical absorption effects, thereby reducing the scattering efficiency and distorting the vibrational response of nearby r8 regions. Third, the effect of laser heating cannot be ignored. Localized heating during Raman measurements could have induced partial phase transitions or further disorder, exacerbating the broadening of the Raman peaks. High-pressure conditions combined with laser-induced temperature rise may have driven transitions from the r8 phase to other metastable or disordered phases, overlapping with the original Raman features and further complicating the spectrum.

In summary, we investigated the high-pressure phase transformation of the $Si_{0.29}Ge_{0.71}$ alloy. In situ synchrotron XRD and micro-Raman measurements revealed that the dc → β-Sn phase transformation occurred at 12.1 GPa, and the β-Sn single phase was obtained at 15.2 GPa. Upon depressurization, the r8 phase appeared at 8.4 GPa. When depressurized to ambient pressure, bc8 and residual r8 and dc phases are present. No appreciable Raman peak was observed up to 4.1 GPa, but weak Raman peaks appeared at ~283 cm^{-1} and ~396 cm^{-1} at ambient pressure. First-principles calculations using DFPT showed that these observed peaks were not related to bc8 but rather to hd, indicating that the bc8 → hd phase transformation was induced by laser heating during the Raman measurement.

See the supplementary material for changes in the lattice constant of the r8 phase upon depressurization, changes in the lattice constant of the r8 phase at ambient pressure, the pair distribution functions of the r8, bc8, and hd-$Si_{0.3}Ge_{0.7}$ phases calculated from atomic structures relaxed at fixed experimental volumes using 80-atom SQS cells, and the first peak positions of the total and partial pair distribution functions for the r8, bc8, and hd-$Si_{0.3}Ge_{0.7}$ phases.

The authors would like to thank Prof. Masamichi Kohno of Kyushu University and Prof. Junichiro Shiomi of the University of Tokyo for valuable discussions. We would also like

to thank Ryo Senno, Makoto Tsuchiya, Sho Sugiyama, and Kaiyo Yoshidome for the high-pressure DAC experiments. The high-pressure DAC experiments were performed with the approval of in the Japan Synchrotron Radiation Research Institute (Proposal Nos. 2024A1303 and 2024B1338). This work was supported by JSPS KAKENHI Grant Number JP23K26405.

AUTHOR DECLARATIONS

Conflict of interest

The authors have no conflicts to disclose.

Author Contributions

Yoshifumi Ikoma: Conceptualization (lead); Funding acquisition (lead); Investigation (equal); Supervision (lead); Writing – original draft (lead). **Yuma Sato:** Data curation (equal); Investigation (equal). **Hirokazu Kadobayashi:** Investigation (equal); Methodology (equal); Writing – review & editing (equal). **Saori Kawaguchi-Imada:** Investigation (equal); Methodology (equal); Writing – review & editing (equal). **Seung Zeon Han:** Funding acquisition (supporting); Writing – review & editing (supporting). **Eun-Ae Choi:** Formal analysis (lead); Investigation (equal); Writing – review & editing (equal). **Yasutomo Arai:** Investigation (equal); Writing – review & editing (equal).

DATA AVAILABILITY

The data that support the findings of this study are available from the corresponding author upon reasonable request.

REFERENCES

1. B. D. Malone and M. L. Cohen, Phys. Rev. B **86**, 054101 (2012).
2. B. Haberl, T. A. Strobel, and J. E. Bradby, Appl. Phys. Rev. **3**, 040808 (2016).
3. A. Mujica, A. Rubio, A. Muñoz, and R. J. Needs, Rev. Mod. Phys. **75**, 863 (2003).
4. S. Yesudhas, V. I. Levitas, F. Lin, K. K. Pandey, and J. S. Smith, Nat. Commun. **15**, 7054 (2024).
5. H. Zhang, H. Liu, K. Wei, O. O. Kurakevych, Y. L. Godec, Z. Liu, J. Martin, M. Guerrette, G. S. Nolas, and T. A. Strobel, Phys. Rev. Lett. **118**, 146601 (2017).
6. B. D. Malone, J. D. Sau, and M. L. Cohen, Phys. Rev. B **78**, 035210 (2008).
7. Z. Zhao, H. Zhang, D. Y. Kim, W. Hu, E. S. Bullock, and T. A. Strobel, Nat. Commun. **8**, 13909 (2017).
8. M. L. Lee, E. A. Fitzgerald, M. T. Bulsara, M. T. Currie, and A. Lochtefeld, J. Appl. Phys. **97**, 011101 (2005).
9. Y. Shiraki and A. Sakai, Surf. Sci. Rep. **59**, 153 (2005).
10. G. A. Slack and M. A. Hussain, J. Appl. Phys. **70**, 2694 (1991).
11. J. Weber and M. I. Alonso, Phys. Rev. B **40**, 5683 (1989).
12. E. M. T. Fadaly, A. Dijkstra, J. R. Suckert, D. Ziss, M. A. J. van Tilburg, C. Mao, Y. Ren, V. T. van Lange, K. Korzun, S. Kölling, M. A. Verheijen, D. Busse, C. Rödl, J. Furthmüller, F. Bechstedt, J. Stangl, J. J. Finley, S. Botti, J. E. M. Haverkort, and E. P. A. M. Bakkers, Nature **580**, 205 (2020).
13. A. Werner, J. A. Sanjurjo, and M. Cardona, Solid State Commun. **44**, 155 (1982).
14. T. Soma, H. Iwanami, and H. Matsuo, Solid State Commun. **42**, 469 (1982).
15. C. R. S. da Silva, P. Venezuela, A. J. R. da Silva, and A. Fazzio, Solid State Commun. **120**, 369373 (2001).
16. M. Y. Lv, Z. W. Chen, R. P. Liu, and W. K. Wang, Solid State Commun. **135**, 749 (2005).
17. A. Hao, L. Zhang, Z. Gao, Y. Zhu, and L. Riping, Phys. Status Solidi B **248**, 1135 (2011).
18. G. Serghiou, G. Ji, M. Koch-Müller, N. Odling, H. J. Reichmann, J. P. Wright, and P.

Johnson, Inorg. Chem. **53**, 5656 (2014).

19. G. Serghiou, N. Odling, H. J. Reichmann, Gang Ji, M. Koch-Müller, D. J. Frost, J. P. Wright, R. Boehler, and W. Morgenroth, Chem. Eur. J. **27**, 14217 (2021).
20. M. Gerin, D. Machon, S. Radescu, S. Le Floch, Y. Le Godec, T. Gaudisson, F. Alabarse, P. Veber, R. Debord, D. Amans, and V. Pischedda, J. Alloys Compd. **954**, 170180 (2023).
21. Y. Ikoma, T. Yamasaki, T. Shimizu, M. Takaira, M. Kohno, Q. Guo, M. R. McCartney, D. J. Smith, Y. Arai, and Z. Horita, Mater. Charact. **169**, 110590 (2020).
22. J. Wagner and M. Núñez-Valdez, Appl. Phys. Lett. **117**, 032105 (2020).
23. K. Kinoshita, Y. Arai, T. Maeda, and O. Nakatsuka, Mater. Sci. Semicond. Process. **70**, 12 (2017).
24. N. Hirao, S. I. Kawaguchi, K. Hirose, K. Shimizu, E. Ohtani, and Y. Ohishi, Matter Radiat. Extremes **5**, 018403 (2020).
25. H. K. Mao, P. M. Bell, J. W. Shaner, and D. J. Steinberg, J. Appl. Phys. **49**, 3276 (1978).
26. Y. Seto, D. Nishio-Hamane, T. Nagai, and N. Sata, Rev. High Pressure Sci. Technol. **20**, 269 (2010).
27. V. Petříček, M. Dušek, and L. Palatinus, Z. Kristallogr. **229**, 345 (2014).
28. G. Kresse and J. Hafner, Phys. Rev. B **47**, 558 (1993).
29. G. Kresse and J. Furthmüller, Phys. Rev. B **54**, 11169 (1996).
30. J. P. Perdew, K. Burke, and M. Ernzerhof, Phys. Rev. Lett. **77**, 3865 (1996).
31. P. E. Blöchl, Phys. Rev. B **50**, 17953 (1994).
32. G. Kresse and D. Joubert, Phys. Rev. B **59**, 1758 (1999).
33. A. Zunger, S. -H. Wei, L. G. Ferreira, and J. E. Bernard, Phys. Rev. Lett. **65**, 353 (1990).
34. A. Van de Walle, P. Tiwary, M. de Jong, D. L. Olmsted, M. Asta, A. Dick, D. Shin, Y. Wang, L. -Q. Chen, and Z.- K. Liu, Calphad **42**, 13 (2013).
35. H. J. Monkhorst and J. D. Pack, Phys. Rev. B **13**, 5188 (1976).
36. L. Vegard, Z. Phys. **5**, 17 (1921).
37. R. J. Nelmes, M. I. McMahon, N. G. Wright, D. R. Allan, and J. S. Loveday, Phys. Rev. B

48, 9883 (1993).

38. S. -Q. Xiao and P. Pirouz, J. Mater. Res. **7,** 1406 (1992).
39. T. Liang, L. Xiong, H. Lou, F. Lan, J. Zhang, Y. Liu, D. Li, Q. Zeng, and Z. Zeng, Scr. Mater. **220**, 114936 (2022).
40. J. P. Dismukes, L. Ekstrom, and R. J. Paff, J. Phys. Chem. **68**, 3021 (1964).
41. H. J. Herzog, "Crystal structure, lattice parameters and liquidus-solidus curve of the SiGe system," in *Properties of Silicon Germanium and SiGe:Carbon*, edited by E. Kasper and K. Lyutovich, (INSPEC, London, 2000), pp. 45–49.
42. F. Pezzoli, L. Martinelli, E. Grilli, M. Guzzi, S. Sanguinetti, M. Bollani, H. D. Chrastina, G. Isella, H. von Kanel, E. Wintersberger, J. Stangl, and G. Bauer, Mater. Sci. Eng. B **124–125**, 127 (2005).
43. R. Yokogawa, S. Sugawa, I. Yonenaga, Y. Arai, and A. Ogura, Jpn. J. Appl. Phys. **63**, 035503 (2024).
44. M. I. Alonso and K. Winer, Phys. Rev. B **39**, 10056 (1989).
45. F. Birch, Phys. Rev. **71**, 809 (1947).
46. M. I. McMahon, R. J. Nelmes, N. G. Wright, and D. R. Allan, Phys. Rev. B **50**, 739 (1994).
47. S. Anzellini, M. T. Wharmby, F. Miozzi, A. Kleppe, D, Daisenberger, and H. Wilhelm, Sci Rep. **9**, 15537 (2019).
48. C. S. Menoni, J. Z. Hu, and I. L. Spain, Phys. Rev. B **34**, 362 (1986).
49. R. H. Wentorf, Jr. and J. S. Kasper, Science **139**, 338 (1963).
50. Y. Ikoma, B. Chon, T. Yamasaki, K. Takahashi, K. Saito, Q. Guo, and Z. Horita, Appl. Phys. Lett. **113**, 101904 (2018).
51. Y. Ikoma, T. Yamasaki, T. Masuda, Y. Tange, Y. Higo, Y. Ohishi, M. R. McCartney, D. J. Smith, and Z. Horita, Philos. Mag. Lett. **101**, 223 (2021).

Figure captions

FIG. 1. (a) Le Bail–refined XRD profile of $Si_{0.29}Ge_{0.71}$ powder at atmospheric pressure. Red circles and the black line correspond to the observed and calculated patterns, respectively. The blue line shows the difference between the observed and calculated patterns. Green ticks indicate theoretical Bragg positions. (b) Raman spectrum of a bulk-crystal $Si_{0.29}Ge_{0.71}$ sample at atmospheric pressure.

FIG. 2. Changes in (a) XRD profiles and (b) Raman spectra of $Si_{0.29}Ge_{0.71}$ powder upon pressurization.

FIG. 3. Fitting curve of the second-order Birch-Murnaghan (BM2) equation of state model for relative volume changes of the dc phase. V_0 is the unit cell volume of the dc phase at atmospheric pressure.

FIG. 4. Changes in (a) XRD profiles and (b) Raman spectra of $Si_{0.29}Ge_{0.71}$ powder upon depressurization.

FIG. 5. DFPT calculations of the Raman-active mode frequencies for (a) the r8-$Si_{0.3}Ge_{0.7}$ phase at 5.6 GPa and (b) the bc8- and hd-$Si_{0.3}Ge_{0.7}$ phases at ambient pressure. (c) Raman spectrum calculated for the hd-$Si_{0.3}Ge_{0.7}$ phase at ambient pressure. The colored bars in (b) and (c) represent the experimentally observed Raman peak positions.

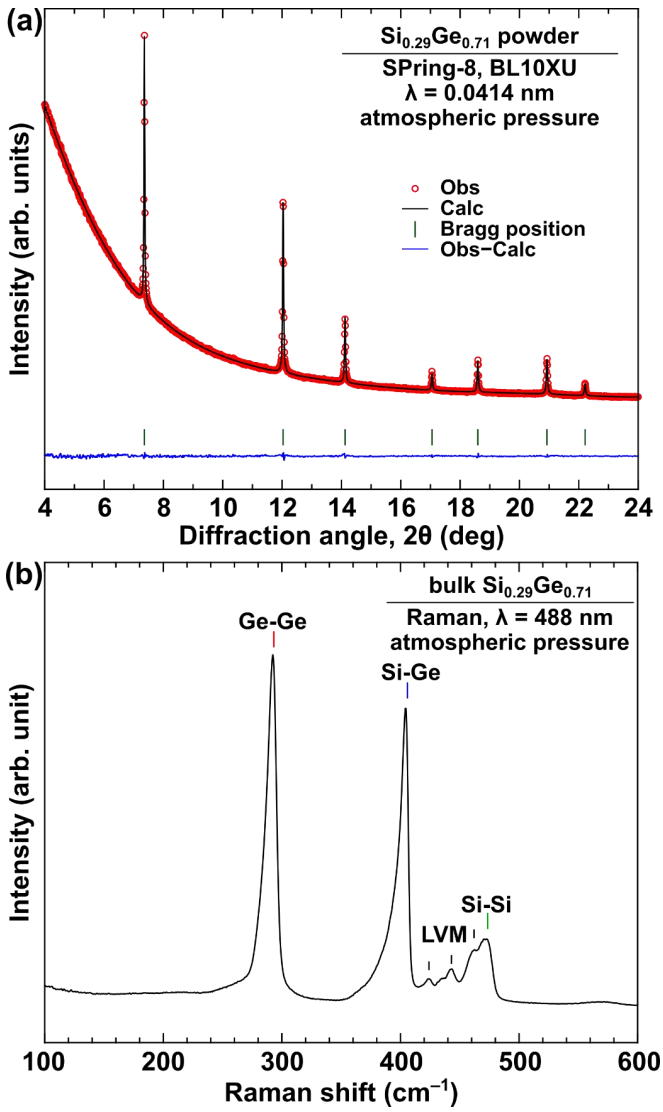

FIG. 1. (a) Le Bail–refined XRD profile of $Si_{0.29}Ge_{0.71}$ powder at atmospheric pressure. Red circles and the black line correspond to the observed and calculated patterns, respectively. The blue line shows the difference between the observed and calculated patterns. Green ticks indicate theoretical Bragg positions. (b) Raman spectrum of a bulk-crystal $Si_{0.29}Ge_{0.71}$ sample at atmospheric pressure.

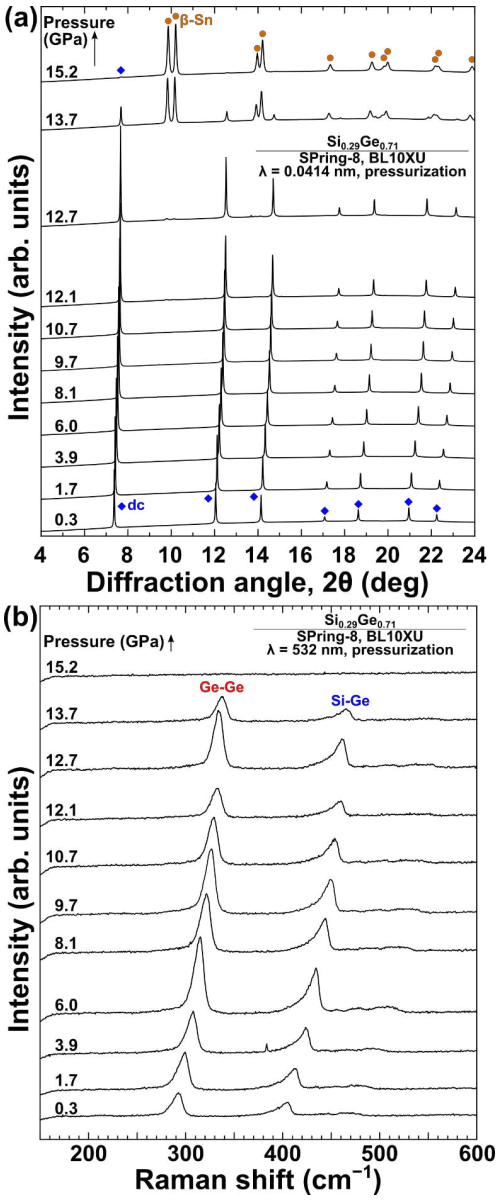

FIG. 2. Changes in (a) XRD profiles and (b) Raman spectra of $Si_{0.29}Ge_{0.71}$ powder upon pressurization.

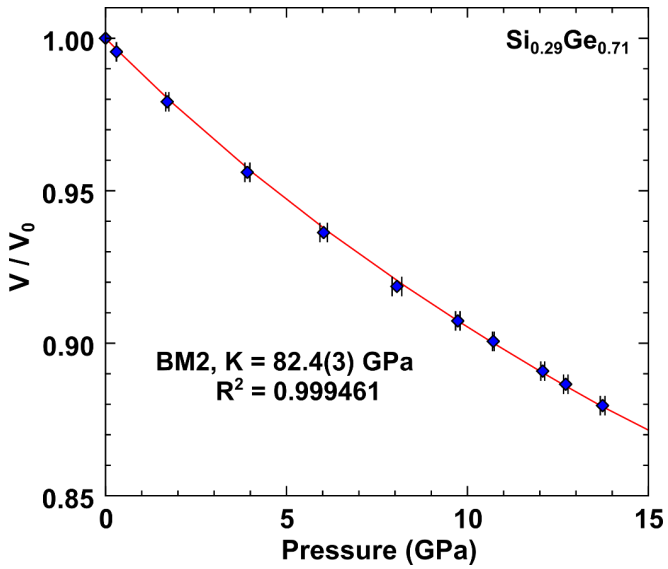

FIG. 3. Fitting curve of the second-order Birch-Murnaghan (BM2) equation of state model for relative volume changes of the dc phase. V_0 is the unit cell volume of the dc phase at atmospheric pressure.

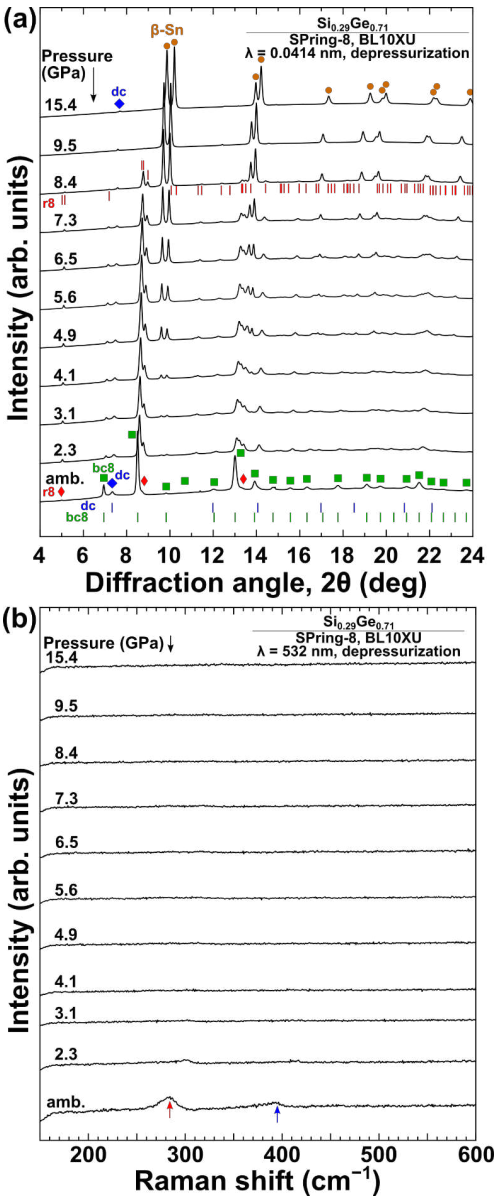

FIG. 4. Changes in (a) XRD profiles and (b) Raman spectra of $Si_{0.29}Ge_{0.71}$ powder upon depressurization.

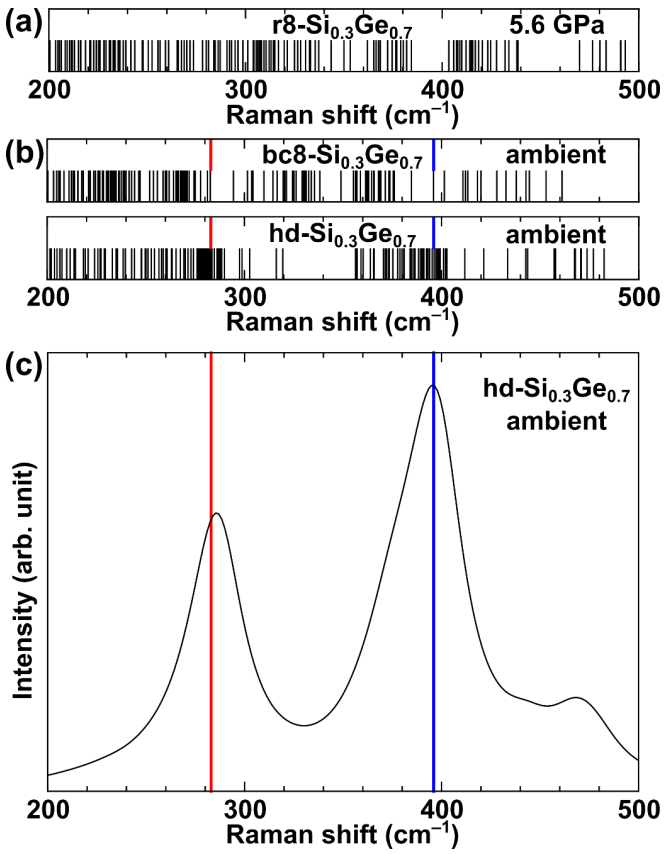

FIG. 5. DFPT calculations of the Raman-active mode frequencies for (a) the r8-$Si_{0.3}Ge_{0.7}$ phase at 5.6 GPa and (b) the bc8- and hd-$Si_{0.3}Ge_{0.7}$ phases at ambient pressure. (c) Raman spectrum calculated for the hd-$Si_{0.3}Ge_{0.7}$ phase at ambient pressure. The colored bars in (b) and (c) represent the experimentally observed Raman peak positions.